
Article:
Zhang, Zhi, Liu, Er, Lu, Xianyang et al. (12 more authors) (2021) Strain-Controlled Spin Wave Excitation and Gilbert Damping in Flexible Co2FeSi Films Activated by Femtosecond Laser Pulse. ADVANCED FUNCTIONAL MATERIALS. 2007211. ISSN 1616-301X

https://doi.org/10.1002/adfm.202007211

Strain-Controlled Spin Wave Excitation and Gilbert damping in Flexible Co_2FeSi Films Activated by Femtosecond Laser Pulse

Zhi Zhang[#], Er Liu[#], Xianyang Lu[#], Wen Zhang[#], Yurong You, Guizhou Xu, Zhan Xu, Ping Kwan Johnny Wong, Yichuan Wang, Bo Liu, Xiaojiang Yu, Andrew Thye Shen Wee, Jing Wu, Yongbing Xu[*], and Feng Xu[*]*

Z. Zhang, Y. You, Z. Zhan, Dr. E. Liu, Dr. G. Xu, Prof. F. Xu
MIIT Key Laboratory of Advanced Metallic and Intermetallic Materials Technology, School of Materials Science and Engineering, Nanjing University of Science and Technology, Nanjing 210094, China
E-mail: ericliu@njust.edu.cn; xufeng@njust.edu.cn
Dr. X. Lu, Dr. B. Liu, Prof. Y. Xu
Jiangsu Provincial Key Laboratory of Advanced Photonic and Electronic Materials, School of Electronic Science and Engineering, Nanjing University, Nanjing 210093, China
York-Nanjing Joint Center (YNJC) for Spintronics and Nanoengineering, Department of Electronic Engineering, University of York, York YO10 5DD, UK
E-mail: ybxu@nju.edu.cn
Prof. W. Zhang
School of Electronics and Information, Northwestern Polytechnical University, 127 West Youyi Road, Xi'an, Shaanxi, 710072, China
Prof. P. K. J. Wong, Prof. A. T. S. Wee
Department of Physics, National University of Singapore, 2 Science Drive 3, Singapore 117542, Singapore
Centre for Advanced 2D Materials and Graphene Research Centre, National University of Singapore, 6 Science Drive 2, Singapore 117546, Singapore
Y. Wang, J.Wu
Department of Physics, University of York, York YO10 5DD, UK
Dr. X. Yu

Singapore Synchrotron Light Source, National University of Singapore, 5 Research Link, Singapore 117603, Singapore

[#] Those authors contribute equally to this work

Keywords: ultrafast magnetization, flexible spintronics, spin wave, X-ray magnetic circular dichroism, Gilbert damping

Abstract

The dynamic respond of magnetic order to optical excitation at sub-picosecond scale has offered an intriguing alternative for magnetism manipulation. Such ultrafast optical manipulation of magnetism has become a fundamental challenging topic with high implications for future spintronics. Here, we explore such manipulation in Co_2FeSi films grown on flexible polyimide substrate, and demonstrate how the magneto-optical interaction can be modified by using strain engineering which in turn triggers the excitation of spin waves including both dipolar and exchange modes. We further show that both the magnetic damping and spin-orbit coupling in Co_2FeSi can be tuned significantly by altering the magnitude and type of applied strain, suggesting an appealing way to manipulate spin wave lifetime. These results develop the optical manipulation magnetism into the field of spin wave dynamics, and open new direction in the application of spin orbitronics and magnonics devices using strain engineering.

1. Introduction

New paradigms enabling high frequency and low consumption data transmission are now in great demands in wireless communication industry.[1] Compared with existing radio-frequency (RF)/microwave technologies, spin waves or magnons are considered as an alternative information carrier, with many remarkable features, such as broad and tunable frequency ranging from MHz to THz with wavelength on micron to sub-nm scales, Joule-heat-free transmission of information over macroscopic distances, and access to wave-based computing concepts.[2-5] Being a collective motion

of magnetic moments, spin waves are in most cases excited and propagate in magnetic films, whose dispersion is dominated by several interactions with different wavelength scale: exchange interaction for short wavelength λ (λ<1 μm, exchange spin waves) and dipolar-dipolar interaction for long wavelength (dipolar or magnetostatic spin waves, MSW).[6] These intriguing yet complex features have triggered both fundamental and device-oriented studies, over the past decades, on the excitation and manipulation of spin waves, in turn leading to magnonics, an emerging research direction under the general field of spintronics.[7-10]

Related to the above is the idea of ultrafast optical manipulation of magnetic order inspired by the discovery of ultrafast demagnetization[11] and all-optical helicity dependent switching (AO-HDS),[12-15] which has led to further investigation of ultrafast magnetization dynamics,[16] exchange interactions,[17,18] subpicosecond demagnetization,[19] *etc*. In those studies, femtosecond pump-probe technique has played an essential role with several advantageous features.[20,21] Fundamentally, it has been demonstrated that femtosecond laser pulses can be utilized to excite spin waves in magnetic materials *via* thermally-mediated processes.[22-24] In contrast to traditional techniques, such as ferromagnetic resonance (FMR) with externally selected microwave-excited spin wave modes,[25,26] ultrafast optical technique activates those mainly determined by intrinsic material properties.[27] The femtosecond temporal resolution of optical pump-probe technique moreover enables the detection of spin waves in much higher frequency regime up to the terahertz. However, the understanding and effective manipulation of spin waves by ultrafast optical technique remain largely

unexplored, given the sophisticated nature of underlying physics involved, such as the coupled interactions between electron, spin and lattice.[20]

Here, we demonstrate the ability to manipulate the ultrafast optically excited spin waves *via* strain applied to Co_2FeSi films grown on flexible polyimide (PI) substrates. The integration of electronic devices with flexible substrates have recently motivated numerous investigations due to its fascinating application in novel portable/wearable devices, such as electronic skin and flexible display.[28-32] The utilization of flexible strain has also unveiled intriguing effect on spin-dependent phenomena, inclusive of exchange bias,[33] interlayer coupling,[34] and perpendicular magnetic anisotropy (PMA).[35] In this work, *via* systematically studying the roles of compressive and tensile strains introduced during film deposition process, we evidence multiple spin waves including both dipolar and exchange modes to be highly tunable. In particular, the magnetic damping α, a decisive factor determining the propagation distance of spin wave, is strongly dependent on the type and magnitude of the applied strain. Using element-specific X-ray magnetic circular dichroism (XMCD) measurements, we provide direct and atomic-level evidence for such strain dependent damping parameter as a result of strain-controlled spin-orbital coupling in Co_2FeSi. The modulation of the spin wave excitation and magnetic damping on flexible thin films as showcased by our pilot study is expected to pave an exciting path toward flexible magnonics devices.

2. Results and Discussion

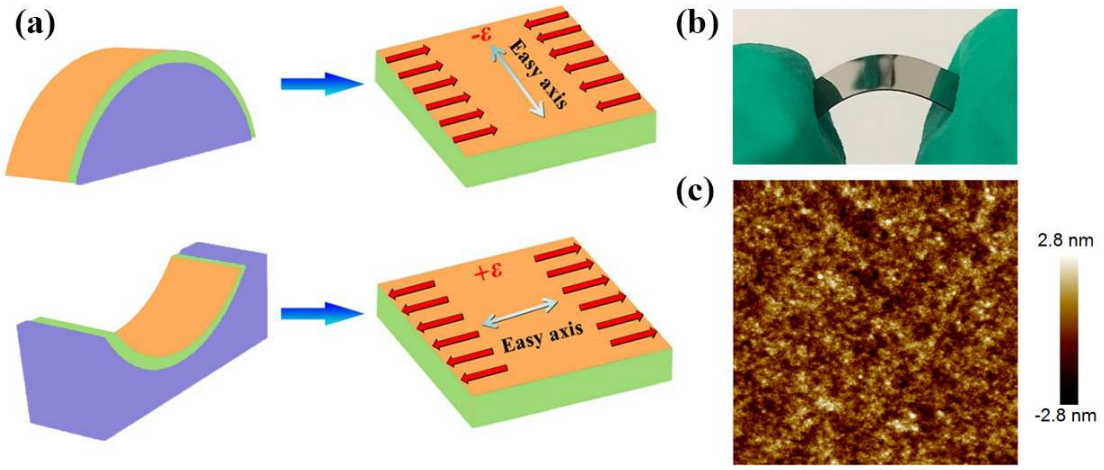

Figure 1. a) Schematic illustration of the strain engineering process: The flexible substrate is fixed on a convex (concave) mold during film deposition to induce a compressive (tensile) strain in the magnetic film. The easy axis of the strain-induced uniaxial anisotropy is perpendicular (parallel) to the compressive (tensile) strain direction. b) Photograph for a Co_2FeSi/Ta film on flexible PI substrate. c) Atomic force microscopy image (1.5 × 1.5 μm^2) for the multilayers without strain.

2.1 Static Magnetic Properties

Strain applied to the Co_2FeSi/Ta film on flexible PI substrate is schematically illustrated in **Figure 1**a. Two types of molds, *i.e.*, convex and concave aluminum molds were employed as a holder for the substrates. The flexible PI substrate was bent and fixed on the mold during film deposition. Upon its removal from the mold followed by subsequent flattening, either a compressive or tensile strain could be introduced into the film. As such, an uniaxial magnetoelastic anisotropy with an easy axis perpendicular (parallel) to the compressive (tensile) strain direction is obtained.[36] The magnitude of such induced strains can be estimated using $\varepsilon = T/2R$, where ε is the compressive or tensile strain, R is the curvature radii of the mold, and T is the total substrate and film

thickness.[37] Here, T is mainly determined by the substrate (125 μm), given its much larger thickness than the multilayer (85 nm). By using molds with different curvature radii, Co_2FeSi/Ta films with the strain ε ranging from -6.26‰ to +6.26‰ have thus been obtained, where the positive (negative) sign denotes the tensile (compressive) strain. A photograph of an as-grown Co_2FeSi/Ta/PI film is illustrated in Figure 1b, evidencing its flexible nature. The surface morphology of a representative film without strain has been examined by atomic force microscopy (AFM) (Figure 1c), indicating a relatively smooth surface with a small root-mean-square roughness of Rq~0.74nm.

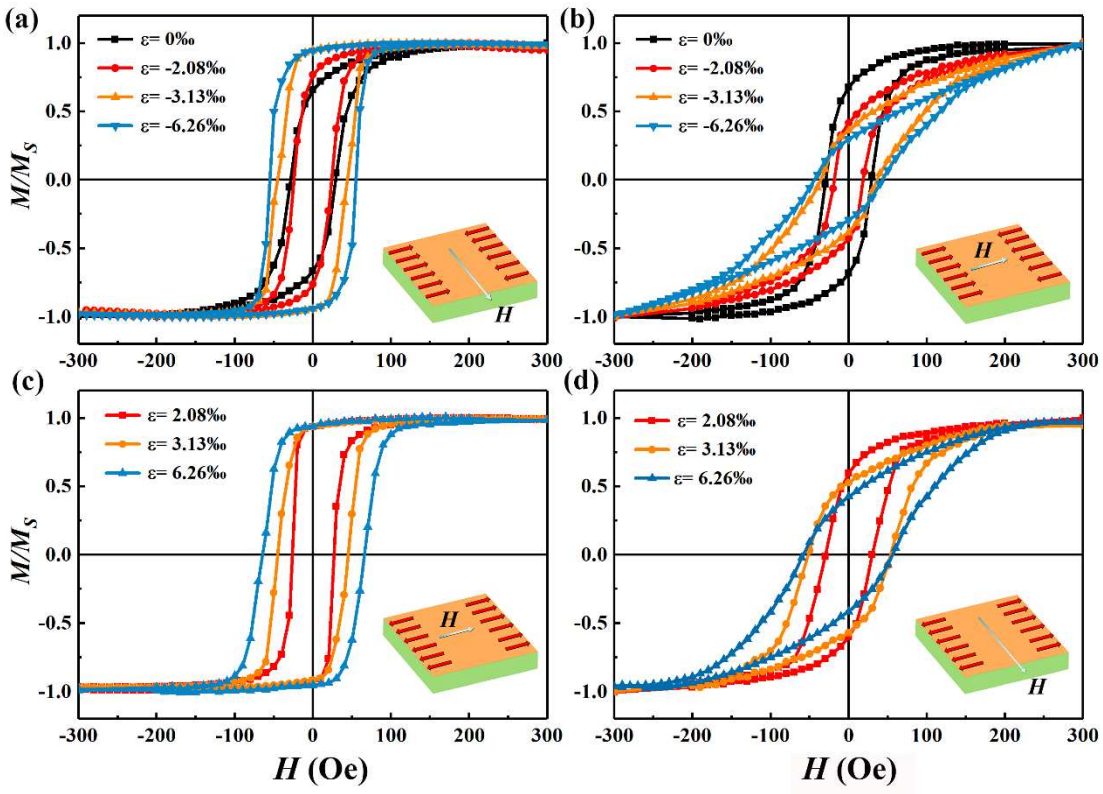

Figure 2. Room temperature magnetic hysteresis loops of Co_2FeSi/Ta films with different compressive a, b) and tensile c, d) strains; the magnetic field was in-plane and applied perpendicular a, d) or parallel to the strain b, c).

The strain effect on the static magnetic properties of the Co_2FeSi films was

characterized by hysteresis-loop measurements with in-plane magnetic field H applied either perpendicular or parallel to the strain direction (**Figure 2**a-d). Notably, the squareness of the loops is seen to increase with the compressive strain when $H \perp \varepsilon$, whereas the loops became more slant when $H // \varepsilon$. Interestingly, opposite strain effect is observed for the tensile strained Co_2FeSi films. These results confirm the existence of a uniaxial anisotropy field H_u in the Co_2FeSi films, with its easy axis being influenced differently by the tensile and compressive strains (*i.e.* $H_u // \varepsilon$ for tensile strain and $H_u \perp \varepsilon$ for compressive strain). We have performed FMR measurements to quantitatively determine the magnitude of such anisotropy field H_u (see supplementary materials).

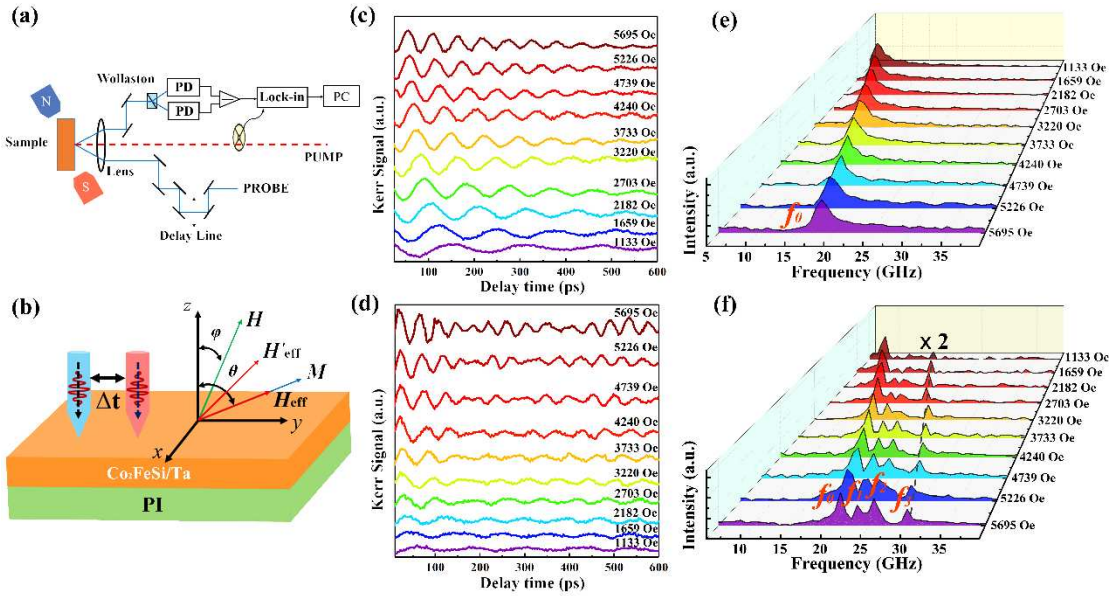

Figure 3. a) Schematic pump-probe TRMOKE setup. b) Sample geometry. c-d) Measured transient Kerr signal of sample with ε = 0 c) and -6.26‰ d). e) and f) FFT spectrums of c) and d). The spin-wave modes in the FFT spectrums are referred to as f_0, f_1, f_2, f_3 mode, respectively.

3. Strain Manipulation of Ultrafast Optical Spin-Wave Excitation

The ultrafast optical excitation of spin waves in the flexible Co_2FeSi films was performed and investigated by time-resolved magneto-optical Kerr effect (TRMOKE) spectroscopy. **Figure 3**a and 3b show the schematic pump-probe TRMOKE setup and the sample geometry, respectively. To promote the magnetic precession, the external magnetic field *H* is applied at an angle φ of 50° away from the sample normal with in-plane projection along the magnetization easy axis, and the precession magnetization *M* at equilibrium direction (denoted by angle θ) is launched by the torque on it as the femtosecond pumping laser transiently changes the orientation of effective field from H_{eff} to H'_{eff}.[38] The detail of the measurement configuration as well as the excitation mechanism can be found in the supplementary materials. Representative TRMOKE results, measured under different *H* fields and at a constant pump fluence of 5.09 mJ cm^{-2}, for the samples with ε = 0 and -6.26‰ are presented in Figures 3c and 3d, respectively. One clearly observes a coherent damping of the magnetization oscillation for the sample with ε = 0, in contrast to the case of the strained film that exhibits a more complicated damping and more resonance modes.[39] Fast Fourier transformation (FFT) of these measured oscillation curves, and their field-dependence are presented in Figures 3e and 3f, respectively, from which strong field dependences of the resonance frequencies and amplitudes of all the observed resonance modes in both types of samples are apparent, thus suggesting their magnetic origin. However, for the sample with ε = 0, we observe only one magnetic resonance or spin-wave mode in the FFT spectra, but there are totally four with frequency ranging from 8.6 GHz to 29.2 GHz for

the strained sample, which we hereafter refer to as f_0, f_1, f_2, f_3 mode, respectively. This finding is interesting and implies the possibility of strain activated ultrafast optical excitation of multimode spin waves.

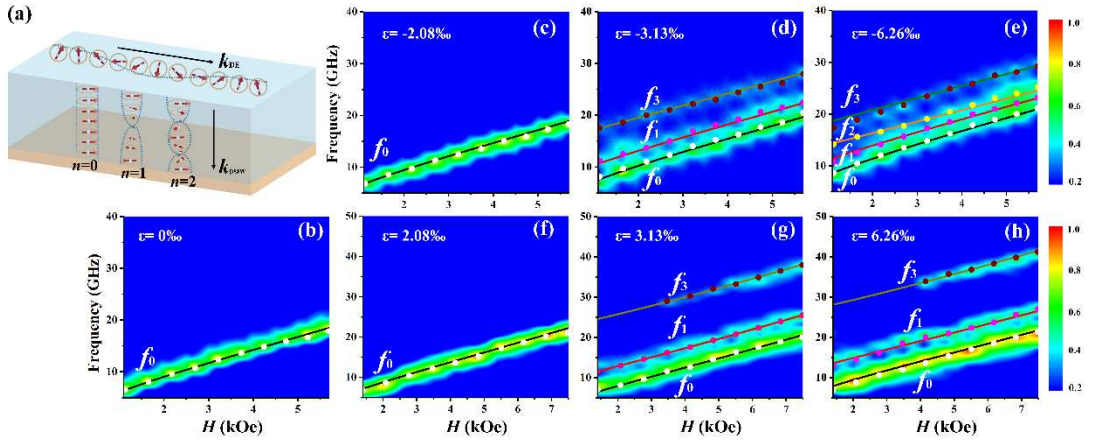

Figure 4 a) Schematic representation of spin-wave modes in a continuous ferromagnetic film. Spin-wave power spectra of Co_2FeSi films with various compressive strains b-e) and tensile strains f-h), experimental frequency data and theoretical fits are denoted by dots (•) and lines (—), respectively.

3.1 Dispersion Analysis: Theoretical Models

To identify these spin-wave modes and their strain dependency, we obtained their dispersions by extracting and fitting the resonance-field dependence of frequency for each mode with different strain configurations. The theoretical dispersion relations for dipolar and exchange spin waves in continuous films under arbitrary effective internal magnetic field can be deduced from the model established by Kalinikos and Slavin.[6] In our work, given that the external magnetic field was applied at φ=50° away from the sample normal with an in-plane projection along the magnetization easy axis, the dispersion equation for angular frequency of exchange-dominated perpendicular standing spin wave (PSSW) mode reads:

$$\omega_{pssw}^2$$

$$= \left[\omega_H + \gamma H_u cos^2\left(\frac{\pi}{2} - \theta\right) + \omega_A n^2\right][\omega_H + \omega_M sin^2\theta + \gamma H_u \cos(\pi - 2\theta) + \omega_A n^2] \quad (1)$$

where ω_H=γHsin $\varphi/sin\theta$, and ω_M=4πγM_S. γ is the gyromagnetic ratio, M_S is the saturation magnetization, and H_u is the strain-induced uniaxial anisotropy field which has been determined by FMR measurements. θ and φ denote the angles of the equilibrium magnetization and external field with respect to the normal of film plane, respectively, as shown in Figure 3b. ω_A=2$\gamma A_{ex}\left(\frac{\pi}{d}\right)^2/M_S$, A_{ex} is the exchange constant, d is the film thickness, and n denotes the order of PSSW mode. If n=0, Equation 1 reduces to the dispersion equation of the Kittle mode as:

$$\omega_{Kittle}^2 = \left[\omega_H + \gamma H_u cos^2\left(\frac{\pi}{2} - \theta\right)\right][\omega_H + \omega_M sin^2\theta + \gamma H_u \cos(\pi - 2\theta)] \quad (2)$$

For the long wavelength dipole spin-wave mode with wave vector $k_{DE}\perp M$ (Damon–Eshbach mode, or DE surface mode), the dispersion equation is given by:

$$\omega_{DE}^2 = {\omega'_H}^2 + \omega_M \omega'_H\left[1 - \frac{cos^2\theta}{k_{DE}d}(1 - e^{-k_{DE}d})\right] + \omega_M^2 \frac{sin^2\theta}{k_{DE}d}(1 - e^{-k_{DE}d})\left[1 - \frac{1}{k_{DE}d}(1 - e^{-k_{DE}d})\right]$$

where ω'_H= $\gamma(H$sin $\varphi/sin\theta + H_u)$.

In our experimental geometry, given the constant value of φ (50°), equilibrium magnetization angle θ can be derived from the following magnetization equilibrium condition,

$$Hsin(\theta - \varphi) - 4\pi M_s sin\theta cos\theta - H_u sin\theta cos\theta =$$

0 (4)

A schematic of different magnetic modes is depicted in **Figure 4**a. One may find that the wavevector of the PSSW modes is perpendicular to the sample plane, and that of DE mode is along the film surface, thereby revealing their different propagation characteristics.

3.2 Dispersion Analysis: Experimental Fit and Discussion

Figure 4 shows the experimental results and theoretical fits for the dispersions of spin-wave modes. It is notable that the number of excited spin waves modes increases with increasing strain regardless of the strain type (compressive or tensile). For Co_2FeSi films with small compressive strain (ε < -3.13‰), only one resonance mode f_0 is observed which can be well fitted by the Kittle equation (Equation 2), as in Figure 4b and 4c. As ε increases to -3.13‰ (Figure 4d), two additional modes f_1 and f_3 with higher frequency and lower amplitude come into play. The dispersions of f_1 and f_3 are well fitted by Equation 1 with setting mode order n to 1 and 2, and the extracted parameter A_{ex}=$(1.10 \pm 0.13) \times 10^{-11}$J/m is comparable to the reported value of Co_2FeSi alloys.[40] Furthermore, the extracted parameters are also valid for the fits to resonance modes f_1 and f_3 in film with $\varepsilon = -6.26‰$ (Figure 4e). As such, f_1 and f_3 in the strained films are identified as the 1st and 2nd order PSSW modes, respectively. However, we find that the dispersion of f_2, an unexpected high frequency mode close to f_1, can be better described by the dipolar DE spin wave mode (Equation 3), rather than the PSSW mode. Such fit yields a reasonable parameter k_{DE}=8.3μm^{-1} in the

wave vector regime of dipolar-interaction-dominated spin waves.[27] It is also worth mentioning that dipolar spin-wave mode with wave vector parallel to magnetization, *i.e.*, backward volume spin wave (BVSW) mode, has not been considered here, since its frequency is expected to be lower than the Kittle mode.[41] On the other hand, for the Co_2FeSi film with $\varepsilon = 6.26‰$, the fitting results suggest only the Kittle mode, 1st order and 2nd order PSSW modes are excited (Figure 4h), even though the ultrafast optical excitation of spin wave manifests similar dependence on the tensile strain for the Co_2FeSi film with less strain (<6.26‰). The results we demonstrated at this point indicate the spin-wave excitation to be well manipulated by strain in the films.

Now we discuss the possible mechanism accounting for the strain-dependent spin-wave excitation. It is well known that spin-wave is a non-uniform magnetic precession or resonance mode, thus either a non-uniform driving field, such as non-uniform microwave magnetic field in FMR system or non-uniform laser field in TRMOKE system, or non-uniformity of magnetic parameters across the sample, is needed to trigger the population of spin-waves.[42-44] In our measurements, the magnetization precession is trigged by the anisotropy field pulse arising from the sample temperature increase due to pump laser pulse absorbed into the films. Given the Co_2FeSi film thickness of 80 nm and also limited optical penetration depth (~10 nm) into the films, the laser field and energy are confined near the film surface. The resulting strong asymmetry of magnetic precession across film thickness will thus favor the excitation of spin-waves,[45-47] especially for the PSSW mode with perpendicular wave vector (parallel to the film thickness direction). However, considering the fact that spin-wave

mode has been observed only in the strained film, the non-uniform laser field is very likely not the only factor causing the observed spin-wave excitation.

Then the key question is why an induced strain is essential for the observed spin-wave excitation in the Co_2FeSi films? One plausible answer is the inhomogeneous distribution of perpendicular magnetic anisotropy field in the Co_2FeSi films arising from the non-uniform strain distribution across the film thickness.[48] As we mentioned above, even though the strain formed by the bending of sample is proportional to the curvature radii, it is not even across the film thickness and so as the uniaxial anisotropy field induced by the strain. This, combined with the non-uniform laser field, might give rise to the excitation of the exchange PSSW mode. For the dipolar DE mode solely observed in the strained film with ε = -6.26‰, it is a surface spin-wave mode with an in-plane wave vector perpendicular to the magnetization ($k_{DE} \perp M$). We also note that the magnetization is perpendicular to the strain direction ($\varepsilon \perp M$) for the film with compressive strain due to the configuration of TRMOKE measurements (the magnetic field was applied with in-plane projection along the magnetization easy axis which is perpendicular to the compressive strain), we thus ascribe the excitation of the DE mode to the non-uniform in-plane distributed anisotropy field along the strain direction owing to the ultrafast heating of atomic lattice. The strain in the Co_2FeSi films distorted the lattice, leading to a less-stable structure compared with films without a strain. Consequently, the lattice vibration (phonon) along the strain direction is easier to be excited due to the ultrafast absorption of photons in the strained film, which in turn leads to the non-uniform in-plane distributed anisotropy field and excitation of the DE

mode. The thermal energy delivered to the lattice is also expected to be maximal at the surface, which decays exponentially into the film due to the limited optical penetration depth. As a surface spin-wave mode, this would also be expected to favor the population of the DE mode. Another possible excitation mechanism of the DE mode is the creation of periodic magnetic ripple pattern in the films.[42,43] We, however, exclude such possibility, because the DE mode remains observable at the magnetic field of up to 5695 Oe, which is much larger than the saturation field.

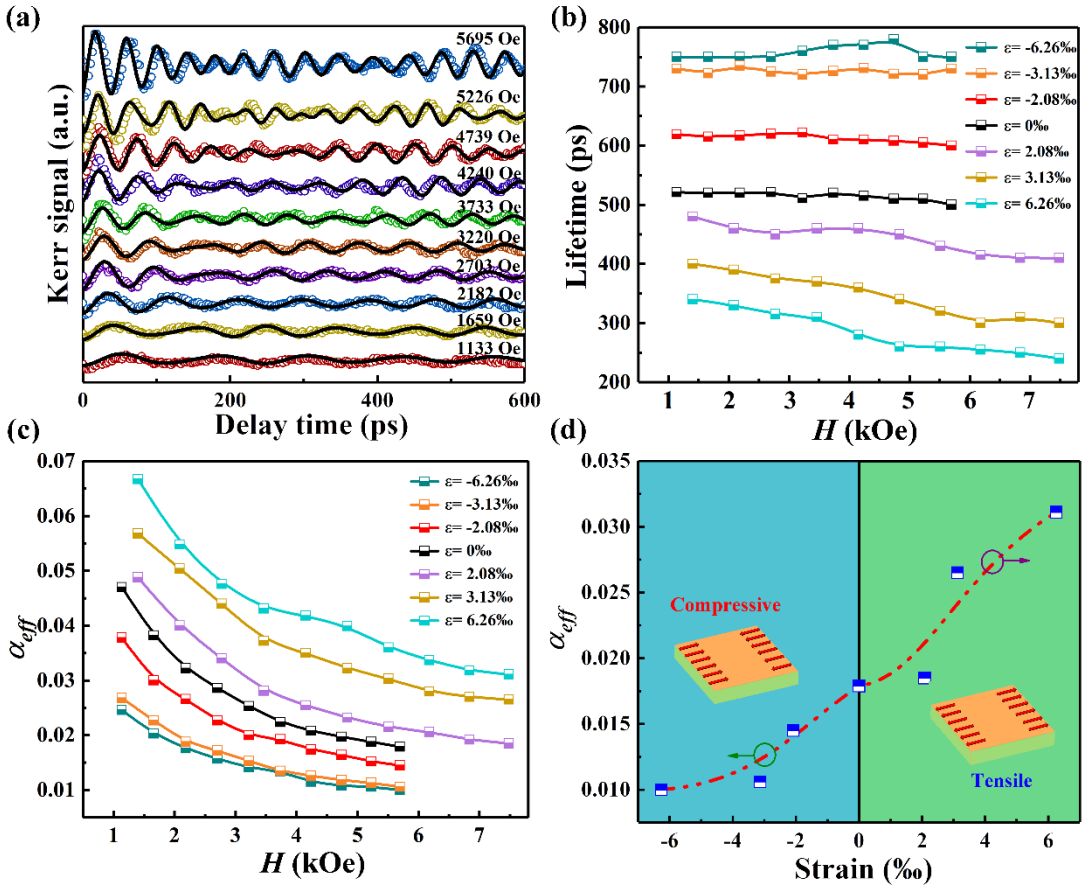

Figure 5 a) Spin-wave dynamics in Figure 3d and their best fits using an exponential sum function. The points show external-field dependence of the lifetime (b) and damping (c) of the Kittle mode in the samples with various strains. Solid lines are the guides to eyes. d) The strain dependence of

the damping at the maximum external field.

4. Strain Control of Gilbert Damping

Compared with the frequency domain measurements of FMR, the time-resolved measurements of TRMOKE allow us to directly observe the magnetization precession in the time domain. The relaxation time of magnetization precession can thus be directly obtained by fitting the TRMOKE spectra, which further enables us to analyze the strain effect on the magnetic damping crucial for the survival lifetime and propagation distance of spin waves in relation to flexible magnonics devices. The time-domain magnetic precession is described based on a phenomenological formula:

$$y(\mathrm{t}) = \sum_{i=1}^{4} A_i \exp\left(-\frac{t}{\tau_i}\right) \sin(2\pi f_i t + \varphi_i) \quad (5)$$

where A_i, τ_i, f_i and φ_i are the amplitude, relaxation (life) time, the precession frequency and the initial phase of magnetization precession, respectively. The TRMOKE spectra for all the samples are fitted with Equation 5. It is seen that the corresponding fit (solid line) for the Co_2FeSi film with ε = -6.26‰ agrees reasonably well with the experimental data (open circles) (**Figure 5**a), from which the lifetime of the spin-wave modes can be extracted. Figure 5b shows the lifetimes of the Kittle modes reflecting the intrinsic damping as the external field approaches infinity.[38] From the Kittle mode lifetime τ,[49,50] one can follow to derive the effective damping constant α_{eff} using the relation $\alpha_{eff} = (2\pi f\tau)^{-1}$. It is noteworthy that the lifetime of the Kittle mode is strongly strain dependent and so as α_{eff}. The external-field and strain dependences of the damping at the maximum external field are shown in Figure 5c and

Figure 5d, respectively. The evolutions of α_{eff} with the applied field under different strains are similar. α_{eff} decreases sharply with the increase of field strength, and almost saturates at high fields for all the samples. The larger α_{eff} at low field arises from the dominantly spatially fluctuating anisotropy field in the effective field which leads to a mixed precession with a damping-enhanced process. While in the high field region, the effect of the anisotropy field becomes weak, since the external field dominates, and hence the reduced contribution of magnetic inhomogeneity to α_{eff}.[50] More importantly, we also notice that α_{eff} shows different dependences on the strain type, as it increases with the tensile strain while decreases with the compressive strain. This unique strain dependent damping behavior is further confirmed by the broadband FMR measurements (Figure S4 in the supplementary materials). Our results strongly indicate that strain is effective in manipulating the spin-wave lifetime and propagation distance, and such an approach is highly desirable for the development of magnonics materials. On the other hand, it remains essential to understand the underlying physics of the strain effect on the magnetic damping. It has been reported that multimode spin-waves excitation can lead to enhanced magnetic damping, since the spin waves provide additional channels for the energy dissipation of the Kittel mode.[49] However, this cannot account for the decrease in damping of the compressive-strained Co_2FeSi film, which implies other strain-related damping mechanism to be explored.

4.1 Mechanism of Strain Effect on the Magnetic Damping

Kambersky's torque-correlation model predicts that the spin orbital coupling ξ_{SO} and density of states near Fermi Level $N(E_{F\pm})$ are main factors contributing to the

magnetic damping.[51] To provide unique insight into the strain effect on ξ_{SO}, we performed element-specific X-ray magnetic circular dichroism (XMCD) measurements for the differently strained Co_2FeSi films, which enables us to extract and separate the orbital and spin moments for each constituting elements in the compound films.[52]

The measurements were taken in the total-electron-yield mode at the grazing incidence (G.I.) of the X-ray beam, with the angle of beam incidence set to 60° with respect to the sample surface normal, as illustrated in **Figure 6**a. Typical X-ray absorption (XA) and XMCD spectra taken at the Co and Fe $L_{2,3}$ edges of the unstrained film are displayed in **Figure 6**b and **6**c, respectively. Those with various strains show highly consistent spectral shapes, which are not displayed here. Note that the Fe XAS has a smaller shoulder beside its L_3 peak, shifted by about 2 eV. This feature probably arises from an *s-d* hybrid state of Fe and Si,[53] which is less pronounced at the Fe L_2 edge.

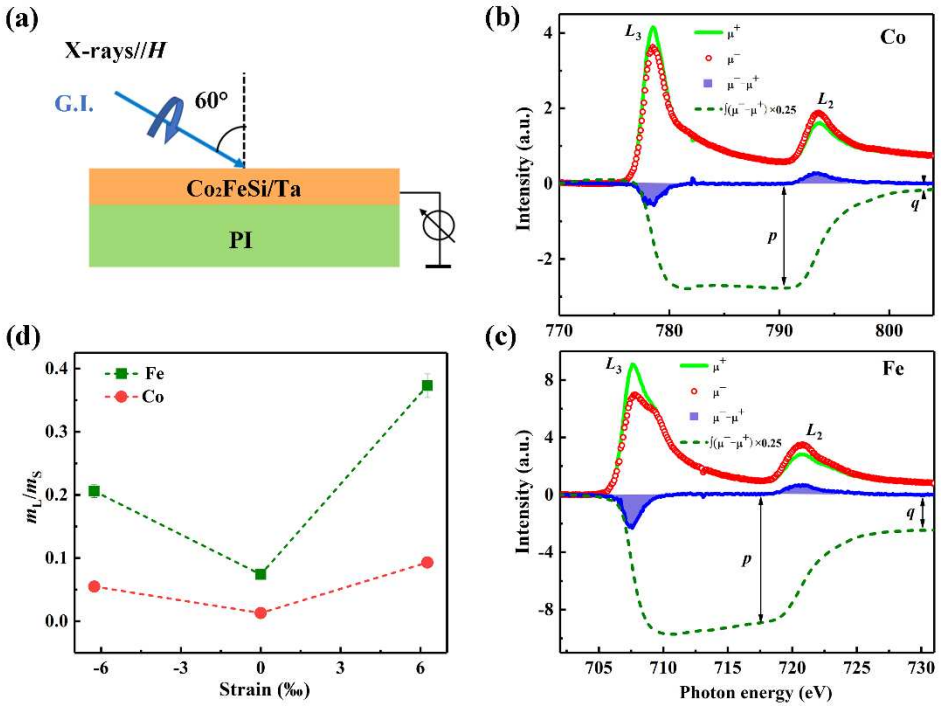

Figure 6 a) Schematic diagram of the experimental geometry for the XMCD measurements with the applied magnetic field along the X-ray incidence direction, and a grazing incidence (GI, $\gamma = 60°$) of the X-ray beam. b, c) Typical XA and XMCD spectra at the Co and Fe $L_{2,3}$ edges, respectively, of the unstrained Co_2FeSi thin films taken at room temperature. A small shoulder beside the L_3 edge of Fe XAS suggests an *s-d* hybrid state of Fe and Si. Integrals of the XMCD (dashed lines) are also shown. d) Orbital-to-spin moment ratio (m_L/m_S) of Co and Fe with different strains of 0, 6.26‰, and -6.26‰, obtained from the XMCD spectra.

In **Figure 6**b and **6**c, μ^+ and μ^- refer to the absorption spectra with the magnetic field parallel and antiparallel to projection of the photon helicity on the sample plane, respectively. The XMCD signal was obtained by (μ^--μ^+). According to the sum rules analysis,[54] the orbital-to-spin moment ratio (m_L/m_S) can be determined by the following equation:

$$m_L/m_S = \frac{q}{3(q-1.5p)}, \quad (6)$$

where p is the integral of the XMCD spectra across the L_3 edge alone, and q is the integral of the XMCD spectra across both edges. m_T corresponds to the magnetic spin dipole moment, arising from the anisotropy of the atomic charge distribution. Here the incident X-ray angle of 60° is close to the magic angle (~55°), where the contribution from m_T can be safely neglected,[55] and accordingly the m_L/m_S ratio of Co and Fe can be approximated using eq (6) as well.

As plotted in **Figure 6**d, we found that both the m_L/m_S ratios of Co and Fe show consistent trends upon the application of strains. Namely, in the non-strain film, the

m_L/m_S ratio is found to be very low, generally due to the quenching effect of the orbitals. Upon the application of strains, the m_L/m_S ratios increase significantly for both compressive and tensile configurations, indicating a strain enhancement ξ_{SO}. The enhanced ξ_{SO} may be induced by the breaking of inversion symmetry in Co_2FeSi lattice due to the strain, which has also been observed in strained semiconductors.[56]

The XMCD measurements unveil the direct experimental evidence on the strain manipulation of spin-orbital coupling, which is promising in the field of spin orbitronics. However, the inconsistent strain dependence of ξ_{SO} and magnetic damping indicates that ξ_{SO} is not the dominent factor for the observed strain dependent damping behavior. Indeed, we also evaluate the strain effect on the density of states of Co_2FeSi using *ab* initio calculations in the supplementary materials. As expected, $N(E_{F\pm})$ is increased by the tensile strain and decreased by the compressive strain, which explains the observed strain dependent damping behavior.

5. Conclusion

In summary, we demonstrate a strain-induced multimode spin-wave excitation approach by using ultrafast optical pump-probe technique in Co_2FeSi films on flexible PI substrate. Multiple spin-wave modes including both dipolar and exchange modes can be excited via introducing strain in the films, and the spin-wave excitation strongly depends on the strain magnitude and type. We argue that the observed spin-wave excitation is triggered by the strain-induced non-uniform magnetic anisotropy field, which arises from the inhomogeneous strain distribution for the exchange PSSW mode,

and from the strain-induced phonons excitation for the dipolar DE mode. Moreover, we reveal that the effective magnetic damping of the Co_2FeSi film manifests opposite dependences on the compressive and tensile strains. It is ascribed to the strain modified $N(E_{F\pm})$ rather than strain enhanced spin-orbital coupling in the Co_2FeSi films, as confirmed by the XMCD and *ab* initio studies. The observed effect not only provides a fascinating approach for enabling optical manipulation of spin wave excitation and dynamics using strain engineering, but also explores the potential of combining magnonics and flexible electronics towards flexible magnonics.

6. Experimental Section

Sample Fabrication. With radio-frequency magnetron sputtering, a series of Co_2FeSi(80nm)/Ta(5nm) films were prepared on 125-μm-thick flexible PI substrates at room temperature with a base pressure lower than 1.5×10^{-5} Pa. The bottom Ta seeding layer was employed to reduce the roughness of the flexible substrates. Before deposition, the substrates were cleaned in ethyl alcohol with ultrasonic agitation for 30 minutes, then dried with nitrogen gas. During deposition, the substrates were bent and fixed on homemade convex or concave aluminum molds with different curvature radii to induce compressive or tensile strains in the multilayers.

Microstructural Characterization. The surface morphology of the thin films was characterized by atomic force microscope (Bruker Multimode 8).

Magnetic Property Measurement. The static magnetic properties were measured by a vibrating sample magnetometer (VSM, Lakeshore 7404-s). The precessional magnetization transient responses were measured by TRMOKE. The laser source used in our setup is a mode-locked amplified Ti: Sapphire laser which emits pulses (800 nm) with a duration of ~60 fs at a repetition frequency of 1000 Hz. The majority of the output laser intensity was used to excite the sample as a pump beam. The remainder passing through a BBO crystal was employed to measure the pump-induced magnetic variation. The time delay between the two beams was achieved by a mechanical delay stage. The detail of the measurement can be found in the supplementary materials.

XMCD Measurement.

The Co and Fe $L_{2,3}$ edge XA/XMCD spectra were collected in total-electron-yield mode, where the sample drain current was recorded as a function of photon energy, with fixed helicity of 80% circularly polarized X-rays and opposite magnetic fields up to ±1 T. The angle of incidence of the photon beam was set to 60° with respect to the sample normal. After normalization to the incident beam intensity, the XMCD spectrum was obtained as the difference between the two XA spectra measured with opposite magnetization directions. Measurements were carried out on (SINS) beamline at the Singapore Synchrotron Light Source.[57,58] All the measurements were performed at room temperature after flattening the bent samples.

Acknowledgements

This work was sponsored by the National Natural Science Foundation of China (Grant No: 51601093, 51571121, 11604148 and 61427812), Fundamental Research Funds for

the Central Universities (Grant No: 30916011345), the Natural Science Foundation of Jiangsu Province (Grant No: BK20160831 and BK20160833), the China Postdoctoral Science Foundation Funded Project (Grant No: 2015M571285, 2016M601811 and 2016M591851), the Postdoctoral Science Foundation Funded Project of Jiangsu Province (Grant No:1601268C), the Key Research & Development Program of Jiangsu Province (Grant No:BE2017102), and Special fund for the transformation of scientific and technological achievements in Jiangsu Province (BA2017121). W.Z., P.K.J.W. and A.T.S.W. acknowledge the financial support from the Singapore Ministry of Education Tier 2 grant (MOE2016-T2-2-110). The authors would like to acknowledge the Singapore Synchrotron Light Source (SSLS) for providing the facility necessary for conducting the research. The Laboratory is a National Research Infrastructure under the National Research Foundation Singapore.

References

[1] A. V. Chumak, V. I. Vasyuchka, A. A. Serga, B. Hillebrands, *Nat. Phys*. **2015**, 11, 453.

[2] A. Bérut, A. Arakelyan, A. Petrosyan, S. Ciliberto, R. Dillenschneider, E. Lutz. *Nature* **2012**, 483, 187.

[3] A. V. Chumak, V. I. Vasyuchka, A. A. Serga, M. P. Kostylev, V. S. Tiberkevich, B. Hillebrands, *Phys. Rev. Lett*. **2012**, 108, 257207.

[4] J. Han, P. Zhang, J. T. Hou, S. A. Siddiqui, L. Liu, *Science*, **2019**, 366, 1121.

[5] K. Vogt, F. Y. Fradin, J. E. Pearson, T. Sebastian, S. D. Bader, B. Hillebrands, A.

Hoffmann, H. Schultheiss, *Nat. Commun*. **2014**, 5, 3727.

[6] B. A. Kalinikos, A. N. Slavin, *J. Phys. C: Solid State Phys.***1986**, 19, 7013.

[7] S. Neusser, D. Grundler, *Adv. Mater*. **2009**, 21, 2927.

[8] H. Fulara, M. Zahedinejad, R. Khymyn, A. A. Awad, S. Muralidhar, M. Dvornik, J. Åkerman, *Sci. Adv*, **2019**, 5, eaax8467.

[9] C. Liu, S. Wu, J. Zhang, J. Chen, J. Ding, J. Ma, Y. Zhang, Y. Sun, S. Tu, H. Wang, P. Liu, C. Li, Y. Jiang, P. Gao, D. Yu, J. Xiao, R. Duine, M. Wu, C. Nan, J. Zhang, H. Yu, *Nat. Nanotech*. **2019**, 14, 691.

[10] D. Karnaushenko, D. Makarov, M. Stöber, D. D. Karnaushenko, S. Baunack, O. G. Schmidt, *Adv. Mater*. **2015**, 27, 880.

[11] E. Beaurepaire, J. C. Merle, A. Daunois, J. Y. Bigot, *Phys. Rev. Lett.* **1996**, 76, 4250.

[12] X. Lu, X. Zou, D. Hinzke, T. Liu, Y. Wang, T. Cheng, J. Wu, T. A. Ostler, J. Cai, U. Nowak, R. W. Chantrell, Y. Zhai, Y. Xu, *Appl. Phys. Lett.* **2018**, 113, 032405.

[13] C. D. Stanciu, F. Hansteen, A. V. Kimel, A. Kirilyuk, A. Tsukamoto, A. Itoh, and Th. Rasing, *Phys. Rev. Lett*. **2007**, 99, 047601.

[14] C-H. Lambert, S. Mangin, B. S. D. Ch. S. Varaprasad, Y. K. Takahashi, M. Hehn, M. Cinchetti, G. Malinowski, K. Hono, Y. Fainman, M. Aeschlimann, E. E. Fullerton, *Science* **2014**, 345, 1337.

[15] S. Mangin, M. Gottwald, C-H. Lambert, D. Steil, V. Uhlíř, L. Pang, M. Hehn, S. Alebrand, M. Cinchetti, G. Malinowski, Y. Fainman, M. Aeschlimann, E. E. Fullerton, *Nat. Mater*. **2014**, 13, 286.

[16] A. M. Kalashnikova, A. V. Kimel, R. V. Pisarev, V. N. Gridnev, P. A. Usachev, A. Kirilyuk, Th. Rasing, *Phys. Rev. B* **2008**, 78, 104301.

[17] A. Mekonnen, M. Cormier, A. V. Kimel, A. Kirilyuk, A. Hrabec, L. Ranno, Th. Rasing, *Phys. Rev. Lett.* **2011**, 107, 117202.

[18] G. Ju, A. V. Nurmikko, R. F. C. Farrow, R. F. Marks, M. J. Carey, B. A. Gurney *Phys. Rev. Lett.* **1999**, 82, 3705.

[19] E. Beaurepaire, J.-C. Merle, A. Daunois, J.-Y. Bigot, *Phys. Rev. Lett.* **1996**, 76, 4250.

[20] A. Kirilyuk, A. V. Kimel, Th. Rasing, *Rev. Mod. Phys.* **2010**, 82, 2731.

[21] B. Liu, W. Niu, Y. Chen, X. Ruan, Z. Tang, X. Wang, W. Liu, L. He, Y. Li, J. Wu, S. Tang, J. Du, R. Zhang, Y. Xu, *Adv. Mater*. **2019**, 31, 1806443.

[22] M. van Kampen, C. Jozsa, J. T. Kohlhepp, P. LeClair, L. Lagae, W. J. M. de Jonge, B. Koopmans, *Phys. Rev. Lett.* **2002**, 88, 227201.

[23] P. Němec, V. Novák, N. Tesarová, E. Rozkotová, H. Reichlová, D. Butkovičová, F. Trojánek, K. Olejník, P. Malý, R. P. Campion, B. L. Gallagher, J. Sinova, T. Jungwirth, *Nat. Commun*. **2013**, 4, 1422.

[24] S. Shihab, L. Thevenard, A. Lemaître, C. Gourdon, *Phys. Rev. B* **2017**, 95, 144411.

[25] S. Neusser, B. Botters, D. Grundler, *Phys. Rev. B* **2008**, 78, 054406.

[26] P. Durrenfeld, F. Gerhard, J. Chico, R. K. Dumas, M. Ranjbar, A. Bergman, L. Bergqvist, A. Delin, C. Gould, L. W. Molenkamp, J. Akerman. *Phys. Rev. B* **2015**, 92, 214424.

[27] B. Lenk, H. Ulrichs, F.Garbs, M. Münzenberg, *Phys. Rep.* **2011**, 507, 107.

[28] M. Melzer, M. Kaltenbrunner, D. Makarov, D. Karnaushenko, D. Karnaushenko, T. Sekitani, T. Someya, O. G. Schmidt, *Nat. Commun*. **2015**, 6, 6080.

[29] T. Vemulkar, R. Mansell, A. Fernández-Pacheco, R. P. Cowburn, *Adv. Funct. Mater*. **2016**, 26, 4704.

[30] D. Shahrjerdi, S. W. Bedell, *Nano Lett*. **2013**, 13, 315.

[31] W. Zeng, L. Shu, Q. Li, S. Chen, F. Wang, X.-M. Tao, *Adv. Mater*. **2014**, 26, 5310.

[32] E. Liu, T. Fache, D. Cespedes-Berrocal, Z. Zhang, S. Petit-Watelot, Stéphane Mangin, F. Xu, J.-C. Rojas-Sánchez, *Phys. Rev. Applied* **2019**, 12, 044074.

[33] Z. Zhang, E. Liu, W. Zhang, P. K. J. Wong, Z. Xu, F. Hu, X. Li, J. Tang, A. T. S. Wee, F. Xu, *ACS Appl. Mater. Interfaces* **2019**, 11, 8258.

[34] Y. Chen, Y. Mei, R. Kaltofen, J. I. Monch, J. Schumann, J. Freudenberger, H. Klauß, O. G. Schmidt, *Adv. Mater*. **2008**, 20, 3224.

[35] Q. Yang, Z. Zhou, L. Wang, H. Zhang, Y. Cheng, Z. Hu, B. Peng, M. Liu, *Adv. Mater*. **2018**, 1800449.

[36] G. Dai, Q. Zhan, H. Yang, Y. Liu, X. Zhang, Z. Zuo, B. Chen, R. Li, *J. Appl. Phys*. **2013**, 114, 173913.

[37] G. Dai, Q. Zhan, Y. Liu, H. Yang, X. Zhang, B. Chen, R. Li, *Appl. Phys. Lett*. **2012**, 100, 122407.

[38] Z. Chen, M. Yi, M. Chen, S. Li, S. Zhou, T. Lai, *Appl. Phys. Lett*. **2012**, 101, 222402.

[39] C. Cheng, K. Meng, S. Li, J. Zhao, T. Lai, *Appl. Phys. Lett*. **2013**, 103, 232406.

[40] S. Trudel, O. Gaier, J. Hamrle, B. Hillebrands, *J. Phys. D: Appl. Phys*. **2010**, 43,

193001.

[41] G. Gubbiotti, G. Carlotti, T. Okuno, T. Shinjo, F. Nizzoli, R. Zivieri, *Phy. Rev. B* **2003**, 68, 184409.

[42] S. J. Hämäläinen, F. Brandl, K. J. A. Franke, D. Grundler, S. van Dijken, *Phys. Rev. Applied* **2017**, 8, 014020.

[43] A. Navabi, C. Chen, A. Barra, M. Yazdani, G. Yu, M. Montazeri, M. Aldosary, J. Li, K.Wong, Q. Hu, J. Shi, G. P. Carman, A. E. Sepulveda, P. K. Amiri, K. L. Wang, *Phys. Rev. Applied* **2017**, 7, 034027.

[44] M. Deb, E. Popova, M. Hehn, N. Keller, S. Petit-Watelot, M. Bargheer, S. Mangin, G. Malinowski, *Phys. Rev. Lett*. **2019**, 123, 027202.

[45] J.-W. Kim, M. Vomir, J.-Y. Bigot, *Phys. Rev. Lett*. **2012**, 109, 166601.

[46] J. Kisielewski, A. Kirilyuk, A. Stupakiewicz, A. Maziewski, A. Kimel, T. Rasing, L. T. Baczewski, and A. Wawro, *Phys. Rev. B* **2012**, 85, 184429.

[47] M. Deb, E. Popova, M. Hehn, N. Keller, S. Mangin, G. Malinowski, *Phys. Rev. B* **2018**, 98, 174407.

[48] X. Qiao, B. Wang, Z. Tang, Y. Shen, H. Yang, J. Wang, Q. Zhan, S. Mao, X. Xu, R. Li, *AIP Advances* **2016**, 6, 056106.

[49] X. Lu, L. J. Atkinson, B. Kuerbanjiang, B. Liu, G. Li, Y. Wang, J. Wang, X. Ruan, J. Wu, R. F. L. Evans, V. K. Lazarov, R. W. Chantrell, Y. Xu, *Appl. Phys. Lett*. **2019**, 114, 192406.

[50] B. Liu, X. Z. Ruan, Z. Y. Wu, H. Q. Tu, J. Du, J. Wu, X. Y. Lu, L. He, R. Zhang, Y. B. Xu, *Appl. Phys. Lett*. **2016**, 109, 042401.

[51] K. Gilmore, Y. U. Idzerda, M. D. Stiles, *Phys. Rev. Lett.* **2007**, 99, 027204.

[52] W. Zhang, P. K. J. Wong, X. Zhou, A. Rath, Z. Huang, H. Wang, S. A. Morton, J. Yuan, L. Zhang, R. Chua, S. Zeng, E. Liu, F. Xu, Ariando, D. H. C. Chua, Y. Feng, G. van der Laan, S. J. Pennycook, Y. Zhai, A. T. S. Wee, *ACS Nano* **2019**, 13, 2253.

[53] M. Meinert, J. Schmalhorst, M. Glas, G. Reiss, E. Arenholz, T. Böhnert, K. Nielsch. *Phys. Rev. B* **2012**, 86, 054420.

[54] J. Stöhr, H. König, *Phys. Rev. Lett.* **1995**, 75, 3748.

[55] H. A. Dürr, G. van der Laan, *Phys. Rev. B* **1996**, 54, R760-R763.

[56] Y. Kato, R. C. Myers, A. C. Gossard, D. D. Awschalom, *Nature* **2004**, 427, 50.

[57] X. Yu, O. Wilhelmi, H. O. Moser, S. V. Vidyarai, X. Gao, A. T. S.Wee, T. Nyunt, H. Qian, H. Zheng, *J. Electron Spectrosc. Relat. Phenom*. **2005**, 1031, 144.

[58] X. Yu, X. Chi, A. T. S. Wee, A. Rusydi, M. B. H. Breese, *Rev. Sci. Instrum.* **2019,** 90, 103902.